

Precession in the inner jet of 3C 345

A. Caproni and Z. Abraham

Instituto de Astronomia, Geofísica e Ciências Atmosféricas, Universidade de São Paulo, R. do Matão 1226, Cidade Universitária, CEP 05508-900, São Paulo, SP, Brazil

acaproni@astro.iag.usp.br

ABSTRACT

VLBI observations have shown that the parsec-jet of 3C 345 is formed by several components, ejected from the core with superluminal velocities and travelling along bent trajectories on the plane of the sky. We interpret the differences in velocity and position angle among the different features at formation time as the result of parsec-scale precession of the relativistic jet and calculate the aperture angle of the precession cone, the angle between the cone axis and the line of sight and the Lorentz factor associated with the jet bulk motion. We assumed a precession period of 10.1 yr, which is one of the *B*-band light curve long-term periods reported in the literature. We propose that boosting of the underlying jet emission, which is time-dependent due to precession, is responsible for this long-term optical variability. Jet precession with periods of several years can be produced in super-massive black hole binary systems, when the secondary black hole is in an orbit non-coplanar with the primary accretion disk, inducing torques in the inner parts of the disk. Assuming that this mechanism is responsible for the jet precession in 3C 345, we estimate upper and lower limits for the masses of the two black holes, as well as their mean separation. We found a correlation between the formation of jet components and the occurrence of strong optical flares, as well as a very strong anti-correlation between the intensity of these flares and the time required for the components to reach the maximum flux density at radio frequencies.

Subject headings: galaxies: active — galaxies: individual: (3C 345) — galaxies: jets — radio continuum: galaxies

1. Introduction

The quasar 3C 345 ($z=0.5928$; Marziani et al. 1996), also known as 1641+399 or 4C 39.48, was optically identified by Goldsmith & Kinman (1965), and it is now known to be the nucleus of an elliptical E3 galaxy (Kirhakos et al. 1999). Strong variability (typical of an OVV object) is found

in its optical light curve, and periodicities of about 5 and 11 yr have been reported (Webb et al. 1988; Kidger 1989; Zhang, Xie & Bai 1998; Zhang et al. 2000), although it has also been suggested that this variability may originate from non-linear and non-stationary stochastic processes (Vio et al. 1991).

The radio flux density has been monitored at several frequencies (Waltman et al. 1991; Aller, Aller & Hughes 1996; Teräsanta et al. 1998). The continuum spectrum is flat up to 10 GHz and gets steeper towards higher frequencies, with spectral index ranging from -0.9 (between $10^{11.9}$ and $10^{13.2}$ Hz) to -1.4 (between $10^{13.2}$ and $10^{15.4}$ Hz) (Bregman et al. 1986). Outbursts have been detected from centimeter to infrared wavelengths (Bregman et al. 1986; Stevens et al. 1996), besides time variable linear polarization at radio and optical frequencies (Moore & Stockman 1981; Bregman et al. 1986; Brown, Roberts & Wardle 1994). In the optical regime, the degree of polarization decreases monotonically toward shorter wavelengths (Sitko, Schmidt & Stein 1985; Smith et al. 1986; Mead et al. 1988; de Diedgo et al. 1994) and in the X-ray range, the source is weak and possibly variable (Halpern 1982; Makino 1989; Worrall & Wilkes 1990).

VLA observations showed a faint halo around a bright core and an extended kiloparsec-jet (Kollgaard, Wardle & Roberts 1989). At parsec-scales, 3C 345 exhibits a stationary core (Bartel et al. 1986; Tang et al. 1990) and a jet with superluminal components, which travel apparently along curved paths with variable velocities (Unwin et al. 1983; Biretta, Moore & Cohen 1986; Zensus, Cohen & Unwin 1995; Ros, Zensus & Lobanov 2000). These characteristics had been interpreted as a result of helical motion of the components along the jet, either in a pure phenomenological model (Qian et al. 1996) or as a consequence of HD or MHD instabilities (e.g., Königl & Choudhuri 1985; Camenzind 1986; Hardee 1987; Qian et al. 1991, 1992; Camenzind & Krockenberger 1992; Steffen et al. 1995; Hardee 2000).

An alternative approach is to assume that the helicoidal appearance of the jet is a consequence of precession. In this case, and considering that the bulk velocity is very large, each plasma element in the jet would move in an almost straight trajectory, defined by the jet direction when this element was ejected. From the observational point of view, superluminal components can be interpreted as these plasma elements, even if they are the results of shock waves propagating along the jet; their velocity should not be very different from the bulk velocity (e.g., Marscher & Gear 1985) and, at least close to their formation epoch, they should reflect the precessing jet direction. Curved trajectories, as found by Zensus, Cohen & Unwin (1995) and Lobanov (1996) in 3C 345, can be due to several reasons: jet instabilities (e.g., Hardee 2000), influence of the external environment (one of the mechanisms proposed by Walker, Benson & Unwin 1987 to explain the bending of the jet in 3C 120), or even the superposition with other components formed at different epochs and moving with different superluminal velocities. In any case, the parameters of the precession model can be completely determined by the superluminal velocities and position angles of the jet components close to their formation epoch.

The parsec-jet precession scenario has already been applied to 3C 279, 3C 273 and OJ 287

(Abraham & Carrara 1998; Abraham & Romero 1999; Abraham 2000), where the velocity variations among components were attributed to differences in the angle between their trajectories and the line of sight. Besides, it was found that the periodic outbursts seen in the optical light curves of 3C 279 and OJ 287 could be due to changes in the boosting parameter (Abraham & Carrara 1998; Abraham 2000). Although this model explained well the behavior of these objects, the precession parameters were obtained from a limited set of data and should probably be revised to include new and more precise data (Homan et al. 2001; Wehrle et al. 2001). We will show in this paper that the variations in the ejection angles and velocities of the jet components of 3C 345 can also be interpreted as the result of parsec-jet precession. Furthermore, we show that the presence of long-term optical variability can be attributed to variable boosting of the non-thermal radiation from the underlying jet.

In Sect.2, we describe the precession model used in this work. In Sect.3, we present the precession model parameters for 3C 345, as well as the influence of precession in the absolute core position shifts due to opacity effects. In Sect.4, we discuss, in the framework of the precession model, other observed characteristics, such as the relation between optical flares and the origin of superluminal components, *B*-band long-term periodic variability, polarimetric observations and dispersion in the apparent angular size of the components. Furthermore, orbital parameters of a possible super-massive black hole binary system in the nucleus of 3C 345 are estimated based on the precession model, with additional constrains from optical continuum and spectroscopic data. Finally, conclusions are presented in Sect.5.

2. Precession model

Let us consider a relativistic jet with bulk velocity β , precessing with a constant angular velocity ω and period P around an axis, forming a conical surface with aperture angle Ω . The cone axis forms an angle ϕ_0 with the line of sight and presents a projected angle η_0 on the plane of the sky. The instantaneous position of the jet is represented by the angles ϕ and η . Their dependence upon the time t' , measured in the comoving frame, can be expressed as (Abraham & Romero 1999; Abraham 2000):

$$\eta(t') = \arctan\left(\frac{y}{x}\right) \quad (1)$$

$$\phi(t') = \arcsin(\sqrt{x^2 + y^2}) \quad (2)$$

with

$$x = (\cos \Omega \sin \phi_0 + \sin \Omega \cos \phi_0 \sin \omega t') \cos \eta_0 - \sin \Omega \cos \omega t' \sin \eta_0 \quad (3)$$

$$y = (\cos \Omega \sin \phi_0 + \sin \Omega \cos \phi_0 \sin \omega t') \sin \eta_0 + \sin \Omega \cos \omega t' \cos \eta_0 \quad (4)$$

The apparent velocity β_{obs} (in units of light speed c) is related to the proper motion of the jet components μ through:

$$\beta_{\text{obs}} = \frac{D_{\text{L}}}{(1+z)} \frac{\mu}{c} \quad (5)$$

where z is the redshift and D_{L} is the luminosity distance, defined as (Carroll, Press & Turner 1992):

$$D_{\text{L}} = \frac{c(1+z)}{H_0} E(\Omega_{\text{M}}, \Omega_{\Lambda}, z) \quad (6)$$

where H_0 is the Hubble constant and E is a function that depends on z and the dimensionless density parameters Ω_{M} and Ω_{Λ} . Throughout the paper, it will be adopted $H_0 = 71 \text{ km s}^{-1} \text{ Mpc}^{-1}$, $\Omega_{\text{M}} = 0.27$ and $\Omega_{\Lambda} = 0.73$, as derived from the recent *WMAP* results (Bennett et al. 2003). In this case, since $\Omega_{\text{M}} + \Omega_{\Lambda} = 1$ the function E is given by (Carroll, Press & Turner 1992):

$$E(\Omega_{\text{M}}, \Omega_{\Lambda}, z) = \int_0^z \frac{dz'}{\sqrt{(1+z')^2(1+\Omega_{\text{M}}z') - z'(2+z')\Omega_{\Lambda}}} \quad (7)$$

For the chosen cosmology, $D_{\text{L}} = 2.47h^{-1} \text{ Gpc}$, with $h = H_0/100$, from which 1 mas yr^{-1} corresponds to an apparent velocity of $24.5h^{-1}c$.

The viewing angle ϕ is not measured directly, but it is related to β_{obs} by:

$$\beta_{\text{obs}} = \frac{\beta \sin[\phi(t')]}{1 - \beta \cos[\phi(t')]} \quad (8)$$

The elapsed time between two events in the observer and comoving frameworks (Δt and $\Delta t'$ respectively) are related by the Doppler factor δ as:

$$\Delta t' = \frac{\delta(\phi, \gamma)}{(1+z)} \Delta t \quad (9)$$

with

$$\delta(\phi, \gamma) = \gamma^{-1} \{1 - \beta \cos[\phi(t')]\}^{-1} \quad (10)$$

and

$$\gamma = (1 - \beta^2)^{-1/2} \quad (11)$$

Thus, given Ω , ϕ_0 , η_0 , β and P , we could predict at any time the observed properties of a precessing jet.

The flux density in the optically thin regime will be boosted according to the expression:

$$S_j(\nu) = S'_j(\nu) \delta(\phi, \gamma)^{p+\alpha} \quad (12)$$

where α is the spectral index ($S_\nu \propto \nu^{-\alpha}$), $p = 2$ for a continuous jet and $p = 3$ for discrete features (Blandford & Königl 1979; Lind & Blandford 1985).

3. Determination of the precession parameters

In this work we used the VLBI data of 3C 345 (core-component distance r , position angle on the plane of the sky η and flux density S_ν) found in the literature, between 5 and 22 GHz, covering almost 20 yr of monitoring (Biretta, Moore & Cohen 1986; Unwin & Wehrle 1992; Unwin et al. 1994; Brown, Roberts & Wardle 1994; Zensus, Cohen & Unwin 1995; Leppänen, Zensus & Diamond 1995; Lobanov 1996; Ros, Zensus & Lobanov 2000). We adopted the emergence epochs for the identified components given in the references, except for C7, for which we ruled out those observations with not clear identification (e.g., C76 in Unwin & Wehrle 1992 and Unwin et al. 1994). As there are no observations of the older components C2 and C3 close to their ejection epoch and C9 has only one reported observation (Ros, Zensus & Lobanov 2000), we did not use them in our fitting. In order to estimate the apparent proper motion μ and position angles of the components, it was assumed quasi-ballistic motions in the inner region of the quasar ($r < 1.0$ mas), since the data show that the trajectories are bent beyond this distance. It is important to emphasize that some components, such as C4 and C5, present variable proper motions and/or position angles even for $r < 1.0$ mas (e.g., Lobanov 1996); in those cases, we have considered only observations taken before the occurrence of significant changes in those quantities. We should note that all the superluminal features became optically thin at distances smaller than 1 mas, since this fact is important for the discussion in Sect. 4.1.

As we used data obtained at different frequencies, it was necessary to take into account opacity effects on the determination of the absolute core position, which introduce frequency-dependent shifts in the core-component distances and proper motions. In the case of a precessing jet, these corrections are time dependent and its magnitude calculated in Appendix A. The parameters involved in this calculation are the integrated synchrotron luminosity L_{syn} , the ratio between upper and lower limits in the relativistic particle energy distribution $\gamma_{\text{max}}/\gamma_{\text{min}}$, the intrinsic jet aperture angle ψ' , and a constant parameter k_e . Following Lobanov (1998), we assumed $\gamma_{\text{max}}/\gamma_{\text{min}} = 100$, $k_e = 1$ and a constant value of 1.58×10^{45} erg s $^{-1}$ for L_{syn} , even though this quantity could be time variable. Finally, we chose $\psi' = 1^\circ$ based on the observed angular size of the jet components as a function of their distances from the core.

Among the parameters discussed in Sect.2, we constrained the precession period P using the B -band photometric data. In fact, Zhang, Xie & Bai (1998) reported a period of 10.1 ± 0.8 yr in the light curve of 3C 345 after application of Jurkevich V_m^2 test (Jurkevich 1971). We assumed that this periodicity is due to variable boosting of the jet emission as the Doppler factor varies with precession (equation [12]).

We adopted an unique Lorentz factor for the bulk motion of all components, compatible with the velocity of the fastest component ($\approx 8.7h^{-1}$ c) given by $\gamma_{\text{min}} = (1 + \beta_{\text{obs}}^2)^{1/2}$ ($\gamma \geq 12.3$ for $h = 0.71$). After fixing γ close to its lower limit, we selected the parameters Ω , ϕ_0 and η_0 that fitted the apparent velocities and position angles of the jet components using equations (1)-(4), with t' as implicit variable. Then, we checked the behaviour of $h\beta_{\text{obs}}$ and η as functions of time through equations (1)-(5), assuming that the position angle of the jet component represents the jet position at the epoch when the component was formed. This procedure was repeated until a good fitting was obtained. For each set of precession parameters, we applied the core opacity shifts to the observational data, which introduced refinements in the kinematic and model parameters. The reduced chi-square value for both $\beta(t)$ and $\eta(t)$, for six superluminal components and three parameters is about 3, most of it due to uncertainties in the position angle η .

In Fig. 1, we present the difference in core position Δr_{core} between 5 and 22 GHz (the frequency range used in our work) as a function of time, calculated with the precession parameters. The mean value obtained for Δr_{core} is 0.26 mas, while its lower and upper limits are respectively 0.21 and 0.31 mas. Lobanov (1996) found an average offset of 0.328 ± 0.020 mas between 1992.45 and 1993.72, in good agreement with our estimate of 0.30 mas for the same interval.

The kinematic parameters of the jet components corrected by opacity effects are presented in Table 1. The quoted errors correspond to the range for which a reasonable fitting for the data could still be found.

The precession parameters that best fitted the data are given in Table 2, while Fig. 2 presents the model fitting in the $(\eta, h\beta_{\text{obs}})$, $(t, h\beta_{\text{obs}})$, (t, η) , (t, δ) and (t, ψ) planes. Lower limits for δ (full triangles) calculated from X-ray observations (Unwin et al. 1983, 1997) are presented in the same figure. The Doppler factors predicted by our model are always above the lower limits imposed

by the X-ray observations. In fact, although other combinations of the precession parameters ϕ_0 , η_0 , Ω and γ also fitted the kinematic data, they resulted in Doppler factors incompatible with the lower limits imposed by the observed X-ray fluxes.

Another consequence of the precession model is a possible dispersion in the component angular sizes. As mentioned before, the observed sizes ψ depend on the angle between the jet and the line of sight (equation [A2]). Observations show a dispersion $11^\circ \leq \psi \leq 45^\circ$ with a mean value of $\langle \psi \rangle = 28^\circ$, at least for distances $r < 1$ mas, where we assumed ballistic motion. These observations, together with the modeled time behaviour of the apparent jet aperture angle (assuming an intrinsic aperture $\psi' = 1^\circ$) are presented in Fig. 2e. The precession model predicts $14^\circ \leq \psi \leq 42^\circ$ and $\langle \psi \rangle = 28^\circ$ and, except for C3a, there is good agreement between the individual observations and the model, which seems to indicate that the jet components have similar intrinsic sizes. If we assume that the time behaviour of ψ is fully described by precession effects, there are several alternatives to explain the discrepancy between the calculated and predicted values for C3a: its intrinsic size is larger than 1° , the estimated value of its apparent size is uncertain due to its low flux density or to its possible relation with C4 (Lobanov 1996), or finally because few observations are available for $r < 1$ mas.

4. Discussion

General results obtained from previous sections are discussed below.

4.1. The optical light curve

In Fig. 3, we show the *B*-band light curve of 3C 345 at the observer's reference frame (Zhang, Xie & Bai 1998). We also show, as a continuous line, the boosted emission of the underlying jet, calculated from equation (12) with $\alpha_{\text{opt}} = 1.66$ (Hagen-Thorn et al. 1996), $p = 2$, the Doppler factor obtained from the precession model and the flux density in the comoving reference frame $S'_j = 7$ nJy, which gives the right values for the observed flux density at epochs 1971-1972 and 1990-1991. The inferred value for the underlying jet flux density is an upper limit, since the total luminosity in the optical band is probably due to the superposition of other processes, such as emission from the accretion disk and from the superluminal components. The existence of a weak underlying jet was already postulated in 3C 279 and OJ 287 (Abraham & Carrara 1998; Abraham 2000).

From the light curve, and whenever observations were available, we were able to associate the emergence of jet components to the occurrence of flares in the optical band¹, even though for the older jet components uncertainties in t_0 lead to a non-unique association. The emergence time of

¹We have considered as optical flares short-time variations (between 5 and 90 days) that introduce changes in the flux density higher than 0.5 mJy.

the superluminal features and their associated flares are explicitly marked in Fig. 3. There we can also see that only flares stronger than a certain limit (about 1.5 mJy) produced detectable superluminal components.

It is not clear whether these optical flares are related to short-lived stages of shock evolution (e.g. Marscher & Gear 1985), or a consequence of some instability produced in the accretion disk (Romero et al. 2000). An unexpected relation between the flare flux density at optical wavelengths and the elapsed time between the epochs of superluminal component ejection and occurrence of maximum flux density at radio frequencies gave us some insight on the origin of these flares. Considering only the interval for which the movement of the jet components is quasi-ballistic, and defining $\Delta T_{\max}(\nu)$ as the the elapsed time between the epoch when the components reach their maximum intensity $t_{\max}(\nu)$ at the observed radio frequency ν and their formation epoch (t_0), we obtain:

$$\Delta T_{\max}(\nu) = t_{\max}(\nu) - t_0 \quad (13)$$

The values of ΔT_{\max} for C3, C3a, C4, C5 and C7, obtained from the flux densities given in Lobanov (1996), are presented in Table 3. We ignored C2 because the maximum occurred before the first observation, and C8 and C9 because few observations are available. We calculated ΔT_{\max} at 22 GHz for all components except for C3 and C3a, for which we used data at 10.7 GHz, because they did not have good time coverage at 22 GHz. The error introduced by the use of a different frequency did not change appreciably our results.

In Fig. 4a, we show the B -band flux densities S_B of the flares associated with the jet components as a function of $\Delta T_{\max}(\nu)$. This plot shows a clear and unexpected anti-correlation between these quantities ($R = -0.97$, where R is the correlation coefficient obtained from a power-law fitting). This kind of correlation was not seen when the maximum radio flux density was considered.

To verify whether this anti-correlation is real or a consequence of variable boosting, it is necessary to make the analysis in the comoving reference frame. As jet components are moving with relativistic velocities, the frequency of the emitted radiation in the comoving frame ν' and the frequency ν measured in the observer's reference frame are related by $\nu = \delta\nu'$. Besides, because time dilation, $\Delta T_{\max}(\nu)$ in the observer's framework is related to $\Delta T'_{\max}(\nu')$, defined in the comoving frame as:

$$\Delta T'_{\max}(\nu') = \Delta T'_{\max}(\nu/\delta) = \delta\Delta T_{\max}(\nu) \quad (14)$$

But what we want is a relation between $\Delta T'_{\max}$ and ΔT_{\max} always at same comoving frequency, for example at frequency ν . Assuming that each component propagates with constant velocity in the comoving reference frame, Abraham (2001) showed that:

$$\Delta T'_{\max}(\nu/\delta) = \delta^{1/b} \Delta T'_{\max}(\nu) \quad (15)$$

where the parameter b depends on the dominating energy loss process (Marscher & Gear 1985). For instance, for jet components in the adiabatic-loss stage, b is given by:

$$b = \frac{2(2s + 1) + 3a(s + 2)}{3(s + 4)} \quad (16)$$

$$s = 2\alpha_r + 1 \quad (17)$$

where α_r is the spectral index at radio wavelengths, and the parameter a depends on the variation of the magnetic field with the distance y' in the jet's reference frame [$B(y') \propto y'^{-a}$]. For $a = 1$, $B_{\perp} \approx B_{\parallel}$ (B_{\perp} and B_{\parallel} are respectively the component of the magnetic field oriented perpendicularly and parallel to the jet axis), while for $a = 2$, $B_{\parallel} \gg B_{\perp}$.

Substituting equation (15) in equation (14), we have that ΔT_{\max} measured in the observer's reference frame and in the comoving frame at same frequency ν are related by:

$$\Delta T_{\max}(\nu) = \delta^{1/b-1} \Delta T'_{\max}(\nu) \quad (18)$$

In Cols. 4 and 5 of Table 3, we present respectively the Doppler factor δ_0 at the formation epoch t_0 and the measured spectral index α_r . Assuming that components are in the adiabatic phase and $a = 1$, we obtained b through equation (16) (Col. 6 of Table 3). With these parameters and equation (18), we determined $\Delta T'_{\max}(\nu)$, displayed in the Col. 7 of Table 3.

The transformation of the optical flux density to its value in the the comoving reference frame depends on the nature of the flare. If it is associated with some kind of instability in the accretion disk, such as perturbations due to the passage of the secondary black hole through the disk (Romero et al. 2000), then the flux density of the flares would not be boosted. As it can be seen in Fig. 4b, the anti-correlation between optical flux density and $\Delta T'_{\max}(\nu)$ is maintained, indicating that the stronger the flare is, the faster the propagation of the perturbations in the disk is.

Other possibility is that the optical flares are produced in the jet in the early stages of the shock evolution. In this case, relativistic corrections are needed and:

$$S_B = \delta^{3+\alpha_{\text{op}}} S'_B \quad (19)$$

where S'_B is the B -band flux density of the flare measured in the comoving frame. The values of S'_B are shown in the last column of Table 3.

In Fig. 4c, we plotted S'_B in terms of $\Delta T'_{\max}(\nu)$. Again, we adopted $\alpha_{\text{opt}} = 1.66$ (Hagen-Thorn et al. 1996). Clearly the remarkable anti-correlation seen in Figs. 4a and b disappears completely, indicating that if the optical flares are short-lived phases of the evolution of superluminal components, the anti-correlation is only a consequence of boosting. However, if the optical flares originate from jet components, we would expect the anti-correlation between maximum flux density in the observer's reference frame and $\Delta T_{\max}(\nu)$ to be observed also at radio frequencies. Since no correlation was found between $\Delta T_{\max}(\nu)$ and maximum flux density at 10.7 or 22 GHz, the scenario where the optical flares are produced in the accretion disk is favoured. It is important to emphasize that the results obtained in this section are not altered if we had considered $a = 2$ in our calculations.

4.2. Polarimetric observations and precession model

Polarimetric interferometry of 3C 345 (Brown, Roberts & Wardle 1994; Leppänen, Zensus & Diamond 1995; Taylor 1998; Ros, Zensus & Lobanov 2000) has shown that the electric field orientation and the fractional polarization vary along its jet. Brown, Roberts & Wardle (1994), observing at 5 GHz, found that the magnetic field is almost aligned with the local jet direction, except at the position of the superluminal features. From observations at 22 GHz, Lobanov & Zensus (1996) and Ros, Zensus & Lobanov (2000) proposed the existence of a transition region where the magnetic field changes its orientation from transverse to longitudinal. In the inner parts, strong shocks would dominate, favouring magnetic field perpendicular to the jet axis, while shocks in the outer region would be weaker, and they would not have too much influence on the magnetic field orientation. The increase of the fractional polarization with distance along the jet would be the result of the superposition, close to the core, of components with different electric field orientations (Ros, Zensus & Lobanov 2000).

If there were alignment between the magnetic field and the underlying jet, as in the case of 3C 345, jet inlet precession would introduce fast time variations in the polarization angle, specially when the viewing angle is small. In fact, at the epochs for which the viewing angle is smallest, our model predicts variations in position angle of 60 degrees during an interval as short as 2.6 yr (Fig. 2c). The vectorial superposition of the electric fields associated with jet components formed during these epochs may lead to the cancellation of the total polarized flux and consequent decrease in the fractional polarization near the core. For larger distances, the differences in apparent velocities between the different components would decrease the superposition and the fractional polarization would be higher.

4.3. Physical parameters of a possible super-massive black hole binary system

The precession period of 10.1 yr assumed in our model is certainly inconsistent with the period of 1000 yr calculated by Lu (1992) using the Lense-Thirring effect (Lense & Thirring 1918), for which jet precession is due to the misalignment between the angular momenta of the accretion disk and of a Kerr black hole. The precession of the accretion disk tidally induced by a secondary black hole in a black hole binary system seems to be a probable precession mechanism (Katz 1980, 1997; Romero et al. 2000). Assuming that last interpretation is correct for 3C 345, we can estimate the physical parameters of the binary system.

Let us consider that the primary and secondary black holes, with masses M_p and M_s respectively, are separated by a distance r_{ps} . From Kepler’s third law, we can relate r_{ps} to the orbital period of the secondary around the primary black hole P_{ps} :

$$r_{ps}^3 = \frac{GM_{tot}}{4\pi^2} P_{ps}^2 \quad (20)$$

where G is the gravitational constant and M_{tot} is the sum of the masses of the two black holes.

In the observer’s reference frame, the orbital period P_{ps}^{obs} will be:

$$P_{ps}^{obs} = (1 + z)P_{ps} \quad (21)$$

If the orbit of the secondary is non-coplanar with the accretion disk, torques could be induced in the inner parts of the accretion disk, producing its precession. Considering that the outer radius of the precessing part of the disk is r_d , Papaloizou & Terquem (1995) and Larwood (1997) calculated its precession period P_d in terms of the masses of the black holes:

$$\frac{2\pi}{P_d}(1 + z) = -\frac{3}{4} \left(\frac{7 - 2n}{5 - n} \right) \frac{GM_s}{r_{ps}^3} \frac{r_d^2}{\sqrt{GM_p r_d}} \cos \theta \quad (22)$$

where n is the polytropic index of the gas (e.g., $n = 3/2$ for a non-relativistic gas and $n = 3$ for the relativistic case) and θ is the inclination of the orbit of the secondary with respect to the plane of the disk.

As it is believed that accretion disks are the main candidates for feeding jets, they are expected to form coupled systems (e.g., Donea & Biermann 1996, 2002). In this case, the jet would precess at the same rate than the disk ($P = P_d$), forming a precession cone with half-opening angle equal to the angle of orbit inclination ($\Omega = \theta$). Thus, equation (22) becomes:

$$\frac{2\pi}{P}(1+z) = -\frac{3}{4} \left(\frac{7-2n}{5-n} \right) \frac{G(M_{\text{tot}} - M_{\text{p}})}{\sqrt{GM_{\text{p}}}} \left(\frac{\sqrt{r_{\text{d}}}}{r_{\text{ps}}} \right)^3 \cos \Omega \quad (23)$$

where M_{s} was replaced by $M_{\text{tot}} - M_{\text{p}}$.

From equation (23), r_{d} can be obtained in terms of M_{p} and M_{tot} by:

$$r_{\text{d}} = \left[-\frac{8\pi}{3} \left(\frac{5-n}{7-2n} \right) \frac{(1+z)}{P \cos \Omega} \frac{r_{\text{ps}}^3}{\sqrt{GM_{\text{tot}}}} \right]^{2/3} \frac{x_{\text{p}}^{1/3}}{(1-x_{\text{p}})^{2/3}} \quad (24)$$

where $x_{\text{p}} = M_{\text{p}}/M_{\text{tot}}$. However, equation (24) is valid only if the disk precesses like a rigid-body, implying that r_{d} must be appreciably smaller than r_{ps} (Papaloizou & Terquem 1995). Thus, if M_{tot} and P_{ps} are previously known, this condition can be used to put an upper limit to the mass of the primary black hole, as well as a lower limit to the secondary mass.

Using the velocity dispersion obtained from the H β line-width and the optical continuum luminosity, Gu, Cao & Jiang (2001) found a mass of $8 \times 10^9 M_{\odot}$ for the central object in 3C 345, which it is assumed to be the value of M_{tot} in this work. In Table 4, we present the separation between the two components of the binary system and upper (lower) limits for the mass of the primary (secondary) black hole for several orbital periods. We show in Fig. 5 the outer radius of the precession disk, as given by equation (24), as a function of x_{p} .

We can rule out orbital periods $P_{\text{ps}}^{\text{obs}} < 4$ yr because, in that case, the time-scale for losses due to gravitational radiation is smaller than about 500 yr (e.g., Begelman, Blandford & Rees 1980; Shapiro & Teukolsky 1983), which would lead to significant changes in the orbit of the secondary and consequently to non-periodic disk precession. In addition, from Table 4 we should not consider periods $P_{\text{ps}}^{\text{obs}} > 6.1$ yr since they correspond to a mass for the secondary black hole larger than that of the primary, which seems to be physically unlikely. For these reasons, the possible ranges of primary and secondary masses are $4 \times 10^9 M_{\odot} \leq M_{\text{p}} \leq 5 \times 10^9 M_{\odot}$ and $3 \times 10^9 M_{\odot} \leq M_{\text{s}} \leq 4 \times 10^9 M_{\odot}$, respectively.

According to Romero et al. (2000), the passage of the secondary black hole through the primary accretion disk can produce density waves and induce shocks in the jet, leading to the formation of the superluminal components. Since the secondary black hole passes through the disk twice per orbit, the maximum efficiency is obtained when each passage produces at least one jet component. Assuming that only one component per passage is formed, the interval between successive ejections of superluminal components, measured in the observer's reference frame $P_{\text{ej}}^{\text{obs}}$, corresponds to $P_{\text{ps}}^{\text{obs}}/2$. If not all the interactions are able to generate a jet component, the observed periodicity would be a multiple of half the orbital period ($P_{\text{ej}}^{\text{obs}} = v P_{\text{ps}}^{\text{obs}}/2$, with $v = 1, 2, 3, \dots$). From the emergence epochs of the jet components, we observe that the median ejection interval is 2.6 yr.

Assuming that this interval corresponds to the maximum ejection efficiency, $P_{\text{ps}}^{\text{obs}} = 5.2$ yr, similar to the period of 5.1 yr found in the 14.5-GHz and B -band light curves (Zhang, Xie & Bai 1998; Kelly et al. 2003). Moreover, if the 2.6-yr ejection period corresponds to twice the half period, we would obtain a full period of less than 4 yr, incompatible with the condition found for stable precession mentioned above.

On the other hand, if each passage of the secondary object through the accretion disk generates multiple components N_c , the relation between $P_{\text{ej}}^{\text{obs}}$ and $P_{\text{ps}}^{\text{obs}}$ is $P_{\text{ej}}^{\text{obs}} = \Upsilon P_{\text{ps}}^{\text{obs}}/2$, where $\Upsilon = v/N_c$. Even in the simplest case where $N_c = 2$, and assuming again $P_{\text{ej}}^{\text{obs}} = 2.6$ yr and $v = 1$, we obtained $P_{\text{ps}}^{\text{obs}} = 10.4$ yr. However, this value for the orbital period corresponds again to a binary system where the secondary black hole is more massive than the primary, so we can also rule out this possibility. Therefore, it is reasonable to conclude that on average, each passage of the secondary through the accretion disk produces one superluminal component.

5. Conclusions

In this work, we used data available in the literature involving the parsec-scale radio structure, which comprise almost twenty years of monitoring of 3C 345. We assumed that all superluminal features have quasi-ballistic motions in the inner regions ($r < 1$ mas).

We showed that, close to the core, the trajectories of the superluminal components can be explained quite well if the jet is precessing with a period of 10.1 yr, one of the B -band periodicities reported by Zhang, Xie & Bai (1998). As a consequence of this, we found a correlation between time variation of the Doppler factor and the optical light curve, indicating that probably the boosted optical emission from the underlying jet is responsible for the B -band long-term periodic variability. An upper limit of 7 nJy for the intrinsic flux density of the underlying jet has been estimated in this work. Lower limits for the Doppler factor calculated previously from X-ray observations (Unwin et al. 1983, 1997) were used as constraints in our model.

In this work, we also analyzed the influence of jet precession in the observed position of the optically thick core at different frequencies (Blandford & Königl 1979; Lobanov 1998). We found that precession introduces a time modulation in the shift corrections, as well as in the direction in which the corrections should be applied. However, core position shifts calculated in this work did not exceed 0.31 mas.

Considering that jet precession in 3C 345 is driven by a secondary super-massive black hole in a non-coplanar orbit around the primary accretion disk and using the total mass of the two black holes derived from the $H\beta$ line-width and optical continuum luminosity (Gu, Cao & Jiang 2001), we estimated the masses of the primary and secondary black holes as $4 \times 10^9 M_\odot \leq M_p \leq 5 \times 10^9 M_\odot$ and $3 \times 10^9 M_\odot \leq M_s \leq 4 \times 10^9 M_\odot$, respectively. In addition, we found that the distance r_{ps} between them should be $5.5 \times 10^{16} \text{ cm} \leq r_{\text{ps}} \leq 7.3 \times 10^{16} \text{ cm}$ and their orbital period $2.5 \text{ yr} \leq P_{\text{ps}} \leq 3.8 \text{ yr}$.

The observed dispersion in the apparent sizes of jet components could be attributed to jet precession and interactions between jet and environment matter. It is corroborated by sudden variations in the radio flux density of the knots when there are changes in their propagation direction. Furthermore, those interactions seem to be responsible for gentle bending seen at distances larger than 1 mas, which could explain also the difference between jet orientation at parsec- and kiloparsec-scales.

We were able to associate the emergence of jet components to the occurrence of flares in the optical band stronger than about 1.5 mJy. We also found an unexpected relation between the flare flux density at optical wavelengths and the elapsed time between the epochs of superluminal component ejection and occurrence of maximum flux density at radio frequencies, which led us to the conclusion that these optical flares are originated in the accretion disk and not in the shock waves seen as superluminal features.

Finally, the complex polarimetric structure of 3C 345 in parsec-scales (Brown, Roberts & Wardle 1994; Leppänen, Zensus & Diamond 1995; Taylor 1998; Ros, Zensus & Lobanov 2000) may be explained by our precession model, when the superposition of jet components with different position angles is considered.

This work was supported by the Brazilian Agencies FAPESP (Proc. 99/10343-3), CNPq and FINEP. We would like to thank the anonymous referee for careful reading of the manuscript and for useful comments and suggestions.

A. Opacity effects on core-component distance in a precessing jet

The kinematic properties of the superluminal components in the jet of 3C 345 depend on the accurate determination of the core-component separation. As pointed out previously (e.g., Blandford & Königl 1979; Lobanov 1996, 1998), the absolute core position r_{core} depends inversely on the frequency when the core is optically thick, which introduces a shift in the core-component separation. Following Blandford & Königl (1979), we can write the absolute core position as:

$$r_{\text{core}}(\nu) = \frac{4.56 \times 10^{-12}(1+z)}{D_L \gamma^2 k_e^{1/3} \psi \sin \phi} \left[\frac{L_{\text{syn}} \sin \phi}{\beta(1 - \beta \cos \phi) \ln(\gamma_{\text{max}}/\gamma_{\text{min}})} \right]^{2/3} \nu^{-1}(\text{mas}) \quad (\text{A1})$$

where z is the redshift, D_L is the luminosity distance (in units of parsec), k_e is a constant ($k_e \leq 1$; Blandford & Königl 1979), L_{syn} is the integrated synchrotron luminosity (in units of erg s⁻¹), while γ_{max} and γ_{min} are related respectively to the upper and lower limits of the energy distribution of the relativistic jet particles. The quantities ψ and ν are respectively the observed aperture angle of the jet (in radians) and the frequency (in Hz); the former is related to the intrinsic jet aperture angle ψ' through (e.g., Mutel et al. 1990):

$$\tan(\psi/2) = \tan(\psi'/2) \cot \phi \quad (\text{A2})$$

The core position shift Δr_{core} between frequencies ν_1 and ν_2 ($\nu_2 \geq \nu_1$) is given by:

$$\Delta r_{\text{core}}(\nu_1, \nu_2) = \frac{4.56 \times 10^{-12}(1+z)}{D_L \gamma^2 k_e^{1/3} \psi \sin \phi} \left[\frac{L_{\text{syn}} \sin \phi}{\beta(1 - \beta \cos \phi) \ln(\gamma_{\text{max}}/\gamma_{\text{min}})} \right]^{2/3} \frac{(\nu_2 - \nu_1)}{\nu_1 \nu_2} (\text{mas}) \quad (\text{A3})$$

Note that if we substitute in equation (A3) a simpler version of equation (A2), $\psi \approx \psi' \csc \theta$, we obtain equation (11) given in Lobanov (1998).

We can see that equation (A3) depends on the angle between the jet and line of sight; in the case of a jet which is precessing, this angle is a function of time, what obviously introduces a time dependency in Δr_{core} . On the other hand, the shifts in the core-component separations do not occur in a fixed direction, but they are oriented according to the direction at which the jet inlet is pointed. As the jet inlet is not resolved by observations, changes in its direction will reflect on changes in the position angle of the core region. Thus, a jet component, located at a distance r from the core and with a position angle η , will have right ascension and declination offsets ($\Delta\alpha$ and $\Delta\delta$ respectively) given by:

$$\Delta\alpha(\nu_1, \nu_2) = r(\nu_1) \sin[\eta(t_{\text{obs}})] - \Delta r_{\text{core}}(\nu_1, \nu_2) \sin[\eta_c(t_{\text{obs}})] \quad (\text{A4a})$$

$$\Delta\delta(\nu_1, \nu_2) = r(\nu_1) \cos[\eta(t_{\text{obs}})] - \Delta r_{\text{core}}(\nu_1, \nu_2) \cos[\eta_c(t_{\text{obs}})] \quad (\text{A4b})$$

where η_c is the position angle of the core at the epoch t_{obs} in which observation is acquired. Once the precession model parameters are known, we are able to determine the second term of the equations (A4a) and (A4b) and correct the component position by core opacity effects; using them, we can determine the corrected core-component distance r_{corr} through:

$$r_{\text{corr}}(\nu_1) = \sqrt{r(\nu_1)^2 + \Delta r_{\text{core}}(\nu_1, \nu_2)^2 - 2r(\nu_1)\Delta r_{\text{core}}(\nu_1, \nu_2) \cos(\eta - \eta_c)} \quad (\text{A5})$$

Note that if $\Delta r_{\text{core}} = 0$, $r_{\text{corr}} = r$. Other particular case is found when there is alignment between the position angles of the core and of the jet component ($\eta = \eta_c$), such that $r_{\text{corr}} = r - \Delta r_{\text{core}}$.

REFERENCES

Abraham, Z., Carrara, E. A. 1998, A&AS, 496, 172.

- Abraham, Z., Romero, G. E. 1999, *A&A*, 344, 61.
- Abraham, Z. 2000, *A&A*, 355, 915.
- Abraham, Z. 2001, in *ASP Conf. Ser. 227, Blazar Demographics and Physics*, ed. P. Padovani & C. M. Urry, (San Francisco: ASP), 108.
- Aller, H. D., Aller, M. F., Hughes, P. A. 1996, in *ASP Conf. Ser. 110, Blazar Continuum Variability*, ed. H. R. Miller, J. R. Webb, J. C. Noble (San Francisco: ASP), 208.
- Bartel, N., Herring, T. A., Ratner, M. I., Shapiro, I. I., Corey, B. E. 1986, *A&A*, 354, 55.
- Begelman, M. C., Blandford, R. D., Rees, M. J. 1980, *Nature*, 287, 307.
- Bennett, C. L., Halpern, M., Hinshaw, G., et al. 2003, *ApJS*, 148, 1.
- Biretta, J. A., Moore, R. L., Cohen, M. H. 1986, *ApJ*, 308, 93.
- Blandford, R. D., Königl, A. 1979, *ApJ*, 232, 34.
- Bregman, J. N., Glassgold, A. E., Huggins, P. J., et al. 1986, *ApJ*, 301, 708.
- Brown, L. F., Roberts, D. H., Wardle, J. F. 1994, *ApJ*, 437, 108.
- Camenzind, M. 1986, *A&A*, 156, 137.
- Camenzind, M., Krockenberger, M. 1992, *A&A*, 255, 59.
- Carroll, S. M., Press, W. H., Turner, E. L. 1992, *ARA&A*, 30, 499.
- de Diego, J. A., Kidger, M. R., Perez, E., Takalo, L. O. 1994, *ApJ*, 424, 76.
- Donea, A. C., Biermann, P. L. 1996, *A&A*, 316, 43.
- Donea, A. C., Biermann, P. L. 2002, *PASA*, 19, 125.
- Goldsmith, D. W., Kinman, T. D. 1965, *ApJ*, 142, 1693.
- Gu, M., Cao, X., Jiang, D. R. 2001, *MNRAS*, 327, 1111.
- Hagen-Thorn, V. A., Marchenko, S. G., Takalo, L. O., Sillanpää, A. 1996, *A&A*, 306, 23.
- Halpern, J. P. 1982, in *X-ray Spectra of Active Galactic Nuclei*, (Harvard Univ., Cambridge, USA: Ph.D. thesis).
- Hardee, P. E. 1987, *ApJ*, 318, 78.
- Hardee, P. E. 2000, *ApJ*, 533, 176.
- Homan, D. C., Ojha, R., Wardle, J. F. C. 2001, *ApJ*, 549, 840.

- Jurkevich, I. N. 1971, *Ap&SS*, 13, 154.
- Katz, J. I. 1980, *ApJ*, 236, L127.
- Katz, J. I. 1997, *ApJ*, 478, 527.
- Kelly, B. C., Hughes, P. A., Aller, H. D., Aller, M. F. 2003, *ApJ*, 591, 695.
- Kidger, M. R. 1989, *A&A*, 226, 9.
- Kirhakos, S., Bahcall, J. N., Schneider, D. P., Jerome, K. 1999, *ApJ*, 520, 67.
- Kollgaard, R. I., Wardle, J. F. C., Roberts, D. H. 1989, *ApJ*, 97, 1550.
- Königl, A., Choudhuri, A. R. 1985, *ApJ*, 289, 173.
- Larwood, J. D. 1997, *MNRAS*, 290, 490.
- Lense, J., Thirring, H. 1918, *Phys. Z.*, 19, 156.
- Leppänen, K. J., Zensus, J. A., Diamond, P. J. 1995, *AJ*, 110, 2479.
- Lind, K. R., Blandford, R. D. 1985, *ApJ*, 295, 358.
- Lobanov, A. P. 1996, in *Physics of the Parsec-Scale Structure in the Quasar 3C 345*, (NMIMT, Socorro, USA: Ph.D. thesis).
- Lobanov, A. P., Zensus, J. A. 1996, in *ASP Conf. Ser. 100, Energy Transport in Radio Galaxies and Quasars*, ed. P. E. Hardee, A. H. Bridle & J. A. Zensus (San Francisco: ASP), 109.
- Lobanov, A. P. 1998, *A&A*, 330, 79.
- Lu, Ju-fu. 1992, *Chin. Astron. Astrophys.*, 16/2, 133.
- Makino, F. 1989, in *AGN and the X-Ray Background, Proc. 23rd ESLAB Symp.*, ed. J. Hunt & B. Battich (Noordwijk: ESA), 803.
- Marscher, A. P., Gear, W. K. 1985, *ApJ*, 298, 114.
- Marziani, P., Sulentic, J. W., Dultzin-Hacyan, D., Calvani, M., Moles, M. 1996, *ApJS*, 104, 37.
- Mead, A. R. G., Brand, P. W. J. L., Hough, J. H., Bailey, J. A. 1988, *MNRAS*, 233, 503.
- Moore, R. L., Stockman, H. S. 1981, *ApJ*, 243, 60.
- Mutel, R. L., Phillips, R. B., Su, B., Bucciferro, R. R. 1990, *ApJ*, 352, 81.
- Papaloizou, J. C. B., Terquem, C., 1995, *MNRAS*, 274, 987.
- Qian, S. J., Witzel, A., Krichbaum, T. P., et al. 1991, *Acta Astron. Sin.*, 32, 369.

- Qian, S. J., Witzel, A., Krichbaum, T. P., et al. 1992, *Chin. Astron. Astrophys.*, 16, 137.
- Qian, S. J., Krichbaum, T. P., Zensus, J. A., Steffen, W., Witzel, A. 1996, *A&A*, 308, 395.
- Romero, G. E., Chajet, L., Abraham, Z., Fan, J. H. 2000, *A&A*, 360, 57.
- Ros, E., Zensus, J. A., Lobanov, A. P. 2000, *A&A*, 354, 55.
- Shapiro, S. L., Teukolsky, S. A. 1983, in *Black Holes, White Dwarfs and Neutron Stars*, John Wiley & Sons, New York, 476.
- Sitko, M. L., Schmidt, G. D., Stein, W. A. 1985, *ApJS*, 59, 323.
- Smith, P. S., Balonek, T. J., Heckart, P. A., Elston, R. 1986, *ApJ*, 305, 484.
- Steffen, W., Zensus, J. A., Krichbaum, T. P., Witzel, A., Qian, S. J. 1995, *A&A*, 302, 335.
- Stevens, J. A., Litchfield, S. J., Robson, E. I., et al. 1996, *ApJ*, 466, 158.
- Tang, G., Bartel, N., Ratner, M. I., et al. 1990, in *Parsec-Scale Radio Jets*, ed. J. A. Zensus & T. J. Pearson (Cambridge: Cambridge Univ. Press), 32.
- Taylor, G. B. 1998, *ApJ*, 506, 637.
- Teräsranta, H., Tornikoski, M., Mujunen, A., et al. 1998, *A&AS*, 132, 305.
- Unwin, S. C., Cohen, M. H., Pearson, T. J., et al. 1983, *ApJ*, 271, 536.
- Unwin, S. C., Wehrle, A. E. 1992, *ApJ*, 398, 74.
- Unwin, S. C., Wehrle, A. E., Urry, C. M., et al. 1994, *ApJ*, 432, 103.
- Unwin, S. C., Wehrle, A. E., Lobanov, A. P., et al. 1997, *ApJ*, 480, 596.
- Vio, R., Cristiani, S., Lessi, O., Salvadori, L. 1991, *ApJ*, 380, 351.
- Walker, R. C., Benson, J. M., Unwin, S. C. 1987, *ApJ*, 316, 546.
- Waltman, E. B., Fiedler, R. L., Johnston, K. J., et al. 1991, *ApJS*, 77, 379.
- Webb, J. R., Smith, A. G., Leacock, R. J., et al. 1988, *AJ*, 95, 374.
- Wehrle, A. E., Piner, B. G., Unwin, S. C., et al. 2001, *ApJS*, 133, 297.
- Worrall, D. M., Wilkes, B. J. 1990, *ApJ*, 360, 396.
- Zensus, J. A., Cohen, M. H., Unwin, S. C. 1995, *ApJ*, 443, 35.
- Zhang, X., Xie, G. Z., Bai, J. M. 1998, *A&A*, 330, 469.

Zhang, X., Xie, G. Z., Bai, J. M., Zhao, G. 2000, Ap&SS, 271, 1.

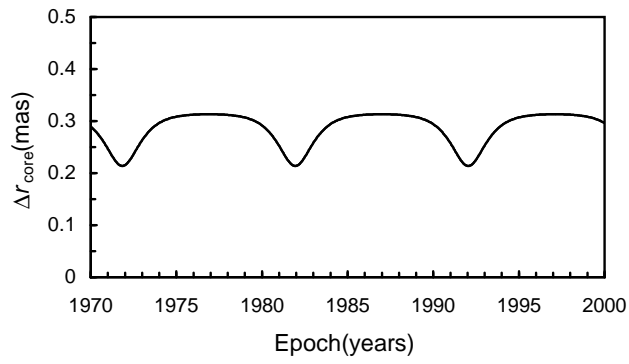


Fig. 1.— Time behaviour due to jet precession of the difference between core position obtained at 5 and 22 GHz.

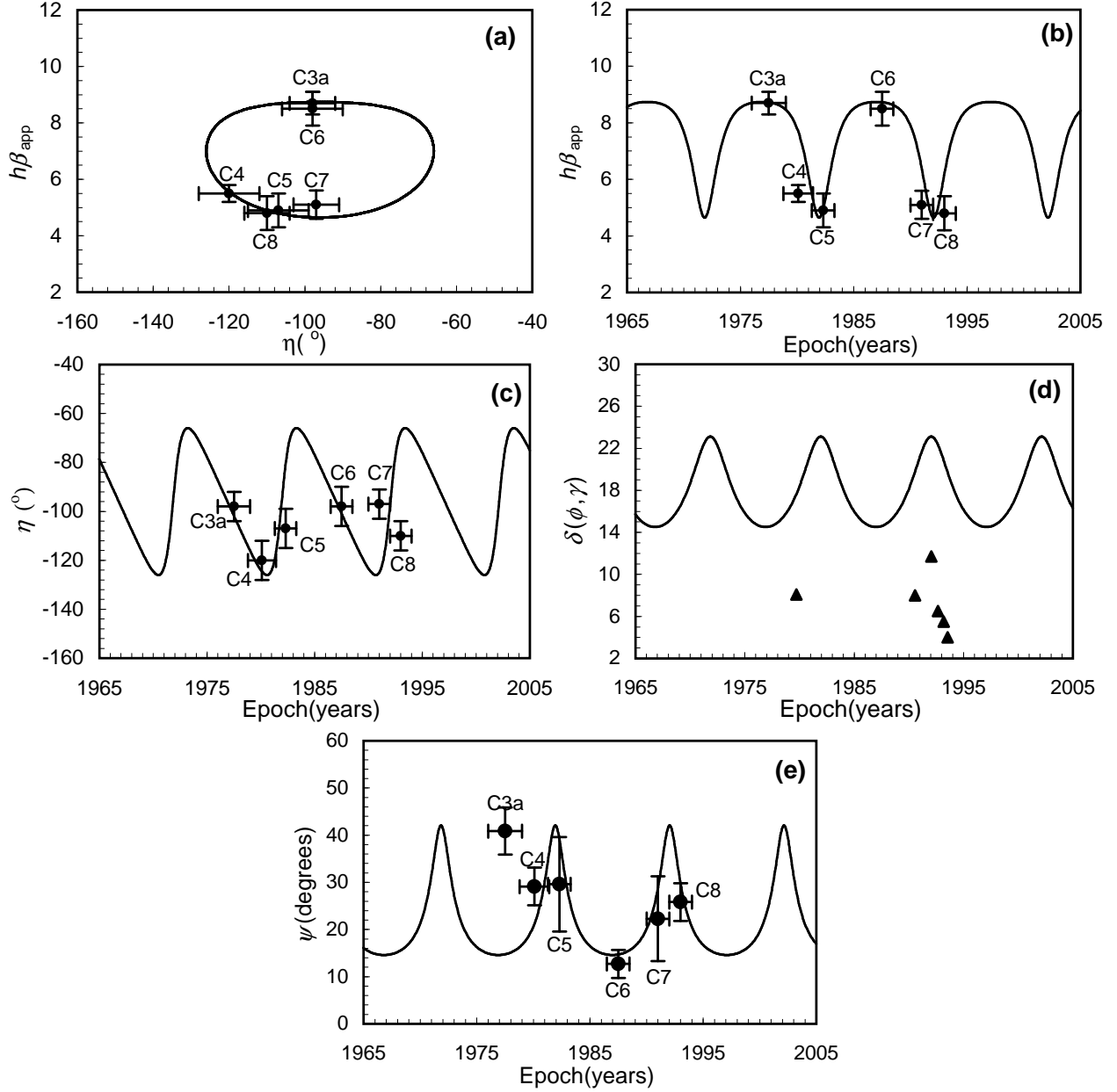


Fig. 2.— Precession model applied to the parsec-scale jet of 3C 345 with model parameters listed in Table 2. (a) - (e): Continuous lines are model predictions on the planes $(\eta, h\beta_{\text{obs}})$, $(t, h\beta_{\text{obs}})$, (t, η) , (t, δ) and (t, ψ) . Full circles and triangles represent, respectively, observations and lower limits for the Doppler boosting factors, calculated from X-ray observations (Unwin et al. 1983, 1997).

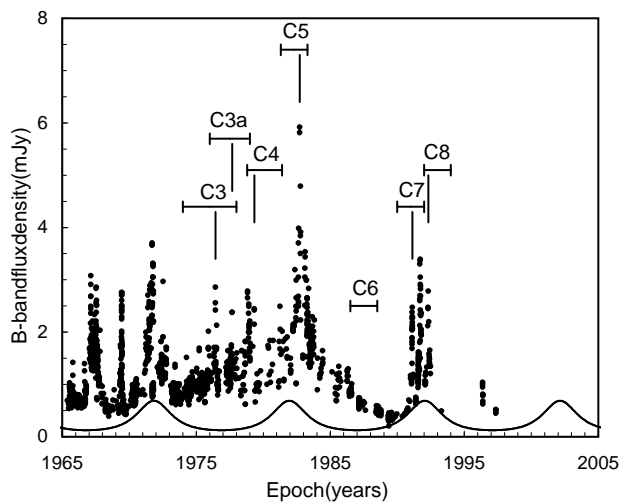


Fig. 3.— *B*-band light curve of 3C 345 (full circles). Solid line represents the expected contribution of the underlying jet. The uncertainty in the emergence epoch of each jet component is represented by the horizontal lines under the component label (see Table 1), while the vertical lines mark the flares that could be associated with these components.

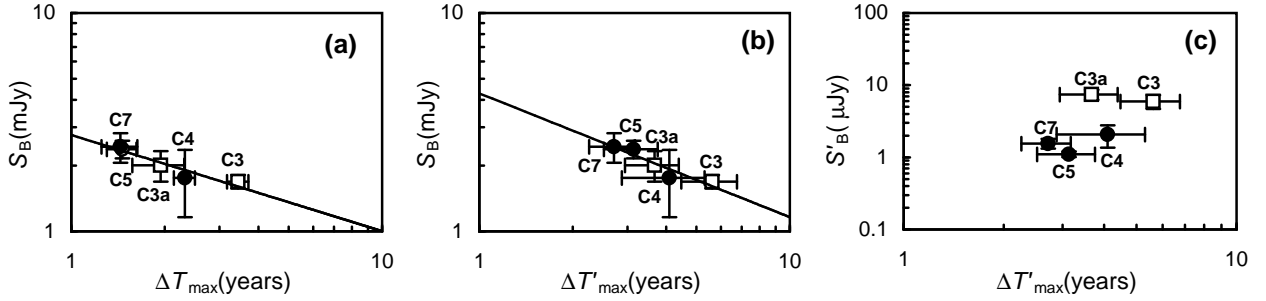


Fig. 4.— Comparison between radio and optical properties of the superluminal components and flares. Filled symbols represent jet components for which 22 GHz radio observations were used, while open symbols correspond to 10.7 GHz observations. **(a)**: B -band flux density of the flares associated with the superluminal features as a function of the elapsed time between the epochs of component ejection and occurrence of maximum flux density at radio frequencies. **(b)**: The same as (a), but as a function of the elapsed time in the comoving jet reference frame. **(c)**: The same as (b), but considering boosting of the optical flux density. The solid line in each plot corresponds to the minimum least squares fitting using power laws.

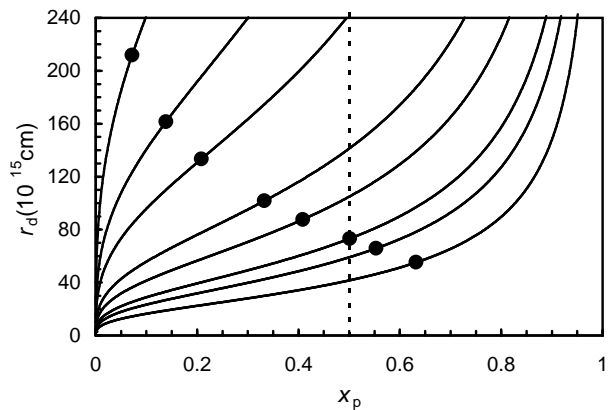


Fig. 5.— Outer radius of the precessing disk as a function of M_p/M_{tot} . Each full line corresponds to a different orbital period, increasing from right to left (see Table 4). The big circles show the values at which the outer radius of the precessing disk equals the separation between the two black holes. The dashed line marks the position in which the masses of the primary and secondary black holes are equal.

Table 1. Parameters of the superluminal components of 3C 345.

Component	t_0 (yr)	μ (mas yr ⁻¹)	$h\beta_{\text{obs}}$	η (°)	OF
C3a	1977.5 ± 1.5	0.355 ± 0.025	8.7 ± 0.4	-98 ± 6	yes
C4	1980.1 ± 1.3	0.225 ± 0.015	5.5 ± 0.3	-120 ± 8	yes ^a
C5	1982.3 ± 1.0	0.200 ± 0.030	4.9 ± 0.6	-107 ± 8	yes
C6	1987.5 ± 1.0	0.347 ± 0.030	8.5 ± 0.6	-98 ± 8	no ^b
C7	1991.0 ± 1.0	0.208 ± 0.025	5.1 ± 0.5	-97 ± 6	yes
C8	1993.0 ± 1.0	0.196 ± 0.030	4.8 ± 0.6	-110 ± 6	yes ^a

Note. — t_0 is the formation epoch, μ and $h\beta_{\text{obs}}$ are, respectively, the proper motion and the apparent velocity in units of light speed c , and η is the ejection angle. Col.OF indicates whether or not there is some optical flare observed in the B -band associated to their ejections.

^aConsidering the uncertainty of t_0 .

^bThere is not any optical observation in the B -band available at this epoch.

Table 2. Parameters of the precession model for the parsec-jet of 3C 120.

P (yr)	^a	γ	Ω (°)	ϕ_0 (°)	η_0 (°)
10.1 ± 0.8 ^b		12.5 ± 0.5	1.3 ± 0.5	2.6 ± 0.5	-96 ± 5

^aMeasured in the framework fixed at the observer.

^bThe quoted error refers to that given by Zhang, Xie & Bai (1998).

Table 3. Optical flares and radio evolution of the superluminal components of 3C 345.

Component	S_{op} (mJy)	ΔT_{max} (yr)	δ_0	α_r	b^a	$\Delta T'_{\text{max}}$ (yr) ^a	S'_{op} (μ Jy)
C3	1.69 ± 0.12	3.44 ± 0.27^b	14.79	0.50 ± 0.35	1.22 ± 0.10	5.6 ± 1.1	6.0 ± 1.3
C3a	2.01 ± 0.32	1.94 ± 0.37^b	14.65	0.76 ± 0.10	1.31 ± 0.03	3.7 ± 0.7	7.4 ± 1.2
C4	1.76 ± 0.60	2.32 ± 0.18^c	18.72	0.55 ± 0.35	1.24 ± 0.15	4.1 ± 1.2	2.1 ± 0.7
C5	2.38 ± 0.22	1.46 ± 0.16^c	22.86	0.80 ± 0.15	1.32 ± 0.09	3.1 ± 0.6	1.1 ± 0.1
C7	2.44 ± 0.38	1.44 ± 0.19^c	21.35	0.61 ± 0.16	1.26 ± 0.06	2.7 ± 0.5	1.6 ± 0.2

Note. — S_{opt} is the flux density of the B -band optical flares. ΔT_{max} is the interval between formation of the jet component and its maximum emission at a given radio frequency (see text). δ_0 is the Doppler factor at the emergence epoch, α_r is the spectral index at radio wavelengths and parameter b , defined by equation (16). Finally, $\Delta T'_{\text{max}}$ and S'_{B} are respectively the interval between formation of the jet component and its maximum emission and the B -band flux density of the flares in the comoving frame.

^aConsidering $a = 1$;

^bAt 10.7 GHz;

^cAt 22 GHz.

Table 4. Parameters of a possible black hole binary system in the inner parts of 3C 345.

$P_{\text{ps}}^{\text{obs}}$ (yr)	P_{ps} (yr)	r_{ps} (cm)	M_{p} (M_{\odot}) ^a	M_{s} (M_{\odot}) ^b
4.0	2.5	5.5×10^{16}	5.0×10^9	3.0×10^9
5.2	3.3	6.6×10^{16}	4.4×10^9	3.6×10^9
6.1	3.8	7.3×10^{16}	4.0×10^9	4.0×10^9
8.0	5.0	8.8×10^{16}	3.2×10^9	4.8×10^9
10.0	6.3	1.0×10^{17}	2.6×10^9	5.4×10^9
15.0	9.4	1.3×10^{17}	1.6×10^9	6.4×10^9
20.0	12.6	1.6×10^{17}	1.0×10^9	7.0×10^9
30.0	18.8	2.1×10^{17}	5.6×10^8	7.4×10^9

^aUpper limit;

^bLower limit.